Titre: Title:	Performance of painted and non-painted non-woven nickel-coated carbon fibers for lightning strike protection of composite aircraft
Auteurs: Authors:	Jean Langot, Etienne Gourcerol, Anamaria Serbescu, David Brassard, Kambiz Chizari, Maxime Lapalme, Alexandra Desautels, Frédéric Sirois, & Daniel Therriault
Date:	2023
Type:	Article de revue / Article
Référence: Citation:	Langot, J., Gourcerol, E., Serbescu, A., Brassard, D., Chizari, K., Lapalme, M., Desautels, A., Sirois, F., & Therriault, D. (2023). Performance of painted and non-painted non-woven nickel-coated carbon fibers for lightning strike protection of composite aircraft. Composites Part A: Applied Science and Manufacturing, 175, 107772 (11 pages). https://doi.org/10.1016/j.compositesa.2023.107772

Performance of painted and non-painted non-woven nickel-coated carbon fibers for lightning strike protection of composite aircraft

Jean Langot[a], Etienne Gourcerol[a], Anamaria Serbescu[a], David Brassard[a], Kambiz Chizari[a], Maxime Lapalme[b], Alexandra Desautels[b], Frédéric Sirois[a], Daniel Therriault[a*]
a: Polytechnique Montreal, 2500 Chem. de Polytechnique, Montréal, QC H3T 1J4, Canada
b: Bell Textron Canada, 12 800 Rue de l'Avenir, Mirabel, QC J7J 1R4, Canada
*daniel.therriault@polymtl.ca (corresponding author)

Abstract

This study investigates the performance of non-woven nickel-coated carbon fibers with varying sheet resistivity as potential solutions for lightning strike protection of composite aircraft, with a focus on the influence of the paint layer on top of the protection. Carbon/epoxy laminates protected by nickel-coated carbon fibers were subjected to lightning strike tests (modified A-waveform), and the heat transfers in the composite were observed using an infrared camera. The damages were analyzed with C-Scan and CT-Scan, and the retention of mechanical properties in bending was characterized via 4-point bending tests. The sheet resistivity, depth and area of damages, retention of mechanical properties, additional cost and weight were then compared to the expanded copper foil currently used in the aerospace industry, with and without a paint layer. With an additional weight of at most 140 g.m^{-2}, nickel-coated carbon fibers are lighter than expanded copper foil (325 g.m^{-2}), while providing 100% of retention of flexural strength after lightning strike, better than the expanded copper foil (90%). However, adding a paint layer decreases the retention of flexural strength to at best 87% when the composite is protected by nickel-coated carbon fibers, but has a very small effect on composites protected by an expanded copper foil.

Index Terms

Lightning strike protection, nickel-coated carbon fiber, expanded copper foil, paint, polymer-matrix composite

I. Introduction

Aircraft are struck by lightning once a year on average [1]. The electrical current of lightning can reach up to 200 kA and generates a plasma channel at 30,000 K [2]. The metallic structures historically used in aircraft fuselage had a very high electrical conductivity and allowed the energy surge of the lightning to diffuse across the fuselage. This avoided energy concentration at the attachment point [3] and mitigated part of the risks associated with lightning strikes. However, metallic fuselages are replaced by lighter composite structures because of stricter emission regulations and for economic reasons. Carbon fiber reinforced polymer (CFRP) composite materials are premium replacement materials but are poor electrical conductors when compared to metals and are prone to significant damages with possible dramatic consequences if left unprotected. Non-metallic solutions such as graphene [4] or buckypaper [5] can be used as lightning strike protection, but their high cost of manufacturing and low electrical conductivity is a disadventage for large aerospace structures. Metal meshes such as expanded copper foils (ECF) are commonly integrated on top of the composite to reduce the sheet resistivity and provide lightning strike protection (LSP) [6]. However, they are relatively expensive and their important weight [7] leads to increased fuel consumption.

In the literature, several solutions were developed to decrease the mass of the lightning strike protection without losing its protective capabilities [8]–[16]. In particular, non-woven (NW) nickel-coated carbon fibers (NCCF) have gained interest in the aerospace community. Table I compares the relevant properties of copper and nickel in terms of LSP. Nickel is less conductive than copper and is more expensive, but has a lower potential of galvanic corrosion with carbon fiber (CF, anodic index of +0.25 V). The difference of anodic index (0.55 V) between nickel and carbon is indeed smaller than between copper and carbon (0.60 V). Nickel has a higher stability at high temperatures than copper because of its higher temperature and latent heat of fusion and vaporization. Moreover, nickel also has an excellent relative magnetic permeability and therefore constitutes a good candidate for electromagnetic shielding applications. Finally, even if copper and nickel have a comparable density, a very thin and homogeneous layer of nickel can be deposited on CF by chemical vapor deposition. This type of protection reduces the sheet resistivity for a potentially lower weight and cost than expanded copper foil. Haynes and Mazas [8] were among the first to use NCCF as lightning strike protection for composites. The damage area after lightning strike of their NCCF protection was similar to expanded metal meshes of equivalent weight. Guo *et al.* [9] showed that composites protected by NCCF had a better retention of mechanical properties after lightning strike than composites protected by expanded metal mesh. Gou *et al.* [10] protected composite panels with a veil of carbon nanofibers and nickel nanostrands, and showed that the protection level of the baseline was related to the sheet resistivity of the veil. However, they did not try to optimize their LSP in terms of weight, cost and performances. Liu *et al.* [11] improved the fracture toughness and through-thickness electrical conductivity of composites by adding a NCCF veil in the middle of the baseline, rather than on top. Zhu *et al.* [12] protected CFRP composites by applying a nickel film on a nylon filter on top of the laminates. Their LSP was slightly lighter than the traditional copper foil, while reaching a similar retention of mechanical properties and area of damage after lightning strike. Nickel was also used in other types of LSP for CFRP composites, such as woven NCCF [13], [17], [18], 3D printed mesh of nickel-coated carbon fiber [16] and nickel-coated carbon nanotubes infused in the matrix [14], [15]. These results are promising and show that NCCF is a serious potential solution for LSP. The protection level is proportional to the conductivity of NCCF [10], which in turn depends on the thickness and therefore the weight of nickel added. The additional weight of LSP has an impact on the aircraft fuel efficiency and should be minimized. Thus, there is a need to optimize

NCCF in terms of protection level, cost and weight.

Composite materials are painted once integrated on the aircraft to protect their outer surface from environmental effects and for aesthetic reasons. However, the paint acts as an insulating layer that disturbs the conductive LSP design. The paint layer constrains the arc root and reduces the diameter of the injection point [19], increasing the current density and the Joule effect in the composite and therefore leading to greater damages. The paint layer can also hinder the evacuation of exhaust gases from matrix pyrolysis, increasing the internal pressure of the composite and enhancing delamination [20]. Overall, the explosion during the lighting strike on painted composites is much more important than on not painted [21]. The depth of damages increases with the paint thickness [22], although very thick paint layers could also protect the composite against heat transfers from the arc. As a result, painting a composite has often a detrimental effect on its resistance to lightning strike; therefore, any LSP should be tested with and without painting before being integrated on an aircraft. However, less than 5% [23] of the authors developing new LSP since 2010 investigated the influence of paint on their performances [24], [25]. In particular, the effect of painting on non-woven nickel coated carbon fibers protections was never investigated.

The objective of this article was to investigate the LSP efficiency of composites protected by non-woven NCCF, with and witout a paint layer on top. In particular, the non-woven NCCF was optimized in terms of protection level, weight and cost. The influence on the protection level of the thickness of nickel coated on carbon fibers and therefore the sheet resistivity of the LSP was also investigated. The samples were exposed to emulated lightning strike with a custom impulse strike setup and compared to a material protected by an expanded copper foil in terms of extent of damages and retention of mechanical properties.

II. Material and Methods

A. Specimen preparation

Four rolls of non-woven NCCF veils with surface resistivity of 0.5, 0.3, 0.1 and 0.04 $\Omega\,\mathrm{sq}^{-1}$ were supplied by Conductive Composites (UT, USA). Each roll consists of a lightweight veil of chopped carbon fibers randomly dispersed and coated with various thickness of nickel to reach the desired conductivity. The thickness of a NCCF veil before integration varies between 0.05 mm (NW0.5) and 0.08 mm (NW0.04). Figure 1 depicts several magnified views of NCCF obtained with SM 7600 TFE Scanning Electron Microscope. Figures 1a) to d) depict how the thickness of nickel coated on a single CF filament is increased to reach the desired conductivity. The conductivity and weight of the NCCF is proportional to the quantity of nickel coated on the carbon fibers.

Figure 2 shows the schematics of the LSP on the composite. The baseline material is composed of 8 plies balanced quasi-isotropic laminates assembled from 0°/90° CF cloth pre-impregnated with epoxy (sequence $[0°\backslash 45°]_{2s}$). The non-woven (NW) veils were integrated on top of the baseline material with the excess resin in the prepreg. The samples were named after the sheet resistivity of the non-woven NCCF. For instance, “NW0.5” indicates a baseline protected by one layer of Non-Woven 0.5 $\Omega\,\mathrm{sq}^{-1}$. A solution composed of two layers of NW0.04 on top of each other was also prepared, named "DNW0.04" (Double-stacked Non-Woven 0.04 $\Omega\,\mathrm{sq}^{-1}$). The excess resin from the prepregs was again used to consolidate the two NW on top of the baseline. Two sets of reference materials were also prepared: unprotected baseline (referred to here as "REF") and baseline protected by an ECF (referred to here as "ECF"). The characteristics of the ECF are indicated in Table II. The laminates were processed, cured using vacuum bagging, pressurized, and heated by autoclave consolidation. In this study, the word "solution" refers to composites protected by a specific type of LSP, and the term "sample" refers to a single panel protected by an LSP. Eight 30 cm × 30 cm (0.093 m^2) samples were prepared per solution studied (for instance, NW0.5, NW0.1, etc). Painted samples were also prepared for each solution (referred to here as "P-REF", "P-ECF", "P-NW" and "P-DNW") to investigate the influence of an insulating coating on the effectiveness of the LSP. The paint consisted of an epoxy-based surface primer. The lateral edges of the panels were sanded to improve the electrical contact between the conductive LSP and the lightning strike emulator's grounding terminal.

B. Sheet resistivity measurements

The sheet resistivity of all non-painted solutions and of NW veils before integration was measured using a 4-point probe method with 5 mm spacing between the electrodes [26]. At least three samples per solution were cut from pristine panels and sanded with a P120 sandpaper. A Keithley 6620 DC current source was used to inject the current from 40 to 60 mA and a Keithley 2182A nanovoltmeter was used to measure the voltage. The sheet resistivity ρ_s was then calculated as following [26]:

$$\rho_s = C\frac{V}{I} \tag{1}$$

where V is the voltage (V), I the current (A), and C a correction factor which depends on the sample dimensions. For 7.5 cm × 7.5 cm samples, a correction factor of $C = 4.3882$ was used.

C. Pyrolysis temperature measurement

Epoxy decomposition has an important role in the generation of damages inflicted to composites exposed to high temperatures [27]. Therefore, the pyrolysis temperature of the composite without LSP was measured via Thermogravimetric Analysis (TGA) by a Mettler-Toledo at atmospheric pressure, following the methodology described in [28]. Three samples ranging from 4 to 17 mg were placed in 70 μl alumina crucibles. As the pyrolysis temperature of epoxy resin usually varies with the heating rate, three different heating rates of 5, 10 and 25 $\mathrm{K\,min}^{-1}$ were used, with one sample per heating rate. Moreover, the TGA was performed under an inert atmosphere (N_2, 60 $\mathrm{ml\,min}^{-1}$) to isolate the matrix pyrolysis from other reactions. Pyrolysis is one of the main cause of damages during the lightning strike [27]. In comparison, carbon fibers and char oxidation have probably a limited influence on the damages, as it is usually much slower than pyrolysis and requires higher temperature ranges [28]. Therefore, oxidation mechanisms were not characterized in this study.

D. Lightning strike emulation tests

The lightning strike tests were performed on six panels (30.5 $\times$ 30.5 cm per solution) with a lightning strike emulator developed at Polytechnique Montreal [29], specifically designed for small scale screening tests. The lightning strike was produced by the discharge of a bank of capacitors charged to 60 kV into a resistor-inductor circuit. The current is injected in the center of samples with a 12.7 mm copper electrode with a tapered conical tip, placed 3 mm above the sample. Diodes are mounted in parallel to the sample to remove the oscillating behavior of the RLC circuit. Therefore, the test waveform mimics the shape of the A-component waveform [30], but the maximum intensity is limited to 40 kA current peak. The objective of the lightning strike emulation tests is to compare different potential LSP, and not to replicate the actual standardized lightning strike test. Then, the sample is connected to the ground by an aluminum frame placed on the sample. The contact surface between the frame and the sample was sanded to ensure good electrical contact. The waveform, peak current, time to peak, time at half peak and action integral of the current in the sample were measured with a Rogowski Current Waveform Transducer CWT 600B and an Lecroy Wavesurfer 422 oscilloscope. A typical A-component waveform produced by the lightning strike emulator is shown on Figure 3. The peak current was the same for all lightning strike tests, ensuring that the post-impact damages on the samples investigated in this study can be compared. However, the right part of the curve, showing the decrease of the current, slightly depended on the electrical conductivity of the sample: the more conductive the sample was, the longer it took to reach half of the maximum current peak. The temperature of the surface of the sample impacted by the lightning strike was recorded with a high-speed infrared camera Telops MS M350. The camera was configured to record in a range between 20°C and 338°C. A light activated trigger allowed the synchronization of 4.5 second recording with the emulated lightning strike. The emissivity of the surface of the composite was measured with a Hemispherical Directional Reflectometer SOC-100 HDR for various temperatures and for a spectral range varying from 3 to 5 μm, from ambient temperature to the maximum operational temperature of the machine (393 K, 120°C). Then, the average emissivity of each sample over these ranges was used as input parameter in the software of the infrared camera to ensure an accurate quantitative measurement of the temperature.

E. Damage analysis

The damages of each sample after lightning strike were assessed as follow: first, the area of damages after lightning strike was analyzed using an ultrasonic C-Scan (TecScan, Gantry), with 5 samples per solution to assess the repeatability of the results. The criteria used to identify a damaged area with the C-Scan was an attenuation of 14 dB, as commonly used in the aerospace industry. Then, 12.7 mm x 90 mm rectangular samples were centered on the damage and cut with water jet (Flow Mach 3, USA) and the depth of damages was analyzed with a 3D X-Ray microscope (xradia 520 versa Zeiss, referred to here as CT-Scan). The CT-Scan was used with a 0.4× objectives, a voltage of 80 kV, a power of 7 W and an exposure time of 1-2 seconds. Only 1 sample per solution was analyzed with the CT-Scan, because CT-Scan analyses are more costly and time consuming.

F. Retention of mechanical properties

The maximum flexural strength and effective elastic modulus in bending after lightning strike were measured with a 4-point bending test, following the methodology described in ASTM D6272-20 [31]. Rectangular samples of 12.7 mm × 90 mm were centered on the damage and cut by water jet on 5 panels for each solution. Other samples were cut in pristine zones and in non-damaged panels to serve as reference. As specified in [31], 5 samples per solution were tested to investigate the repeatability of the tests. The applied force with respect to the mid-span displacement in bending was measured using a universal testing machine (Instron 1362 frame with MTS ReNew controller, load cell capacity of 5 kN, MTS TW-Elite software), on which the damaged area was solicited in tension. The mid-span deflection of the samples was measured by Digital Imaging Correlation or using a displacement gauge (model: MTS 632-06H-30). Loading and support noses of 5 mm in diameter were used. The support and load span were 54.08 and 18.03 mm, respectively. The flexural strength and Young's modulus were calculated with the equations 2 and 3 introduced in ASTM D6272-20 [31], with a support to load span ratio of 1:3 and a length to depth ratio of 32:

$$S = \frac{PL}{bd^2}\left(1 + 4.70D^2/L^2 - 7.04Dd/L^2\right) \tag{2}$$

$$E_B = 0.21L^3m/bd^3 \tag{3}$$

Where S is the flexural strength (MPa), E_B the modulus of elasticity in bending (MPa), P the load at the moment of break (N), L the support span (mm), b the width of beam (mm), d the depth of beam (mm), D the maximum deflection of the center of the beam (mm), m the slope of the tangent at the initial straigth line. S and E_B were calculated using the same material thickness (1.69 mm), as the LSP and paint layer are considered to be non-structural

Finally, the retention of flexural strength and modulus of elasticity in bending were obtained by dividing the properties of damaged panels by the properties of pristine panels. .

III. RESULTS

A. Sample manufacturing and preliminary tests

The additional weight and cost of each solution in comparison to REF (baseline without protection) before painting is summarized in Figure 4. The additional cost was estimated with the data from the suppliers of each LSP. In this study, all panels protected by NW NCCF are cheaper and also significantly lighter than ECF, which is attributed to (i) the very low quantity of nickel coated on carbon fibers, and (ii) to the absence of adhesive necessary to incorporate the non-woven NCCF on the plies below. The absence of adhesive is a significant advantage of the NCCFs when compared to the copper foil. Due to its important thickness ($\sim$ 0.1 mm), the copper foil must be integrated on the baseline with adhesive, inducing an important weight penalty as the use of adhesive for integration contributes in weight around 181 $\mathrm{g\,m^{-2}}$ (more than 50% of the additional weight). On the other hand, NCCF are thinner ($\sim$ 0.05 to 0.08 mm). They can therefore be incorporated on the laminate with only the exceeding resin from the prepreg, without adding adhesive, and do not change significantly the panel thickness after integration (see Table III). This difference of manufacturing process offers a significant weight advantage to NCCF when compared to copper foil. Moreover, regardless of the manufacturing process, the copper foil alone has an additional weight of 146 $\mathrm{g\,m^{-2}}$ and is heavier than all NCCF used in this study (23 to 140 $\mathrm{g\,m^{-2}}$).

It is worth noting that the additional price estimated here is valid for this particular study only and is not normalized by weight or sheet resistivity. It does not imply that nickel solutions are necessarily always cheaper than copper solution of equivalent protective capabilities for actual standardized lightning strike test (200 kA). Moreover, prices could vary significantly if NCCF were used on a large-scale production. Nevertheless, the prices estimated here show that nickel-based solution are not necessarily more expensive than copper-based solution, and can even be cheaper.

The sheet resistivity before painting of each solution are indicated in Table III. The sheet resistivity "before integration" was measured on the NW veils alone before integration on the baseline material, and the sheet resistivity "after integration" was measured on the baseline protected by the NW veils. Overall, all panels protected by nickel solutions are less resistive than REF. It is also worth noting that the surface resistivity of the NW after integration (0.175 to 0.062 $\Omega\,\mathrm{sq}^{-1}$) was lower than the resistivity of NW before integration (0.430 to 0.124 $\Omega\,\mathrm{sq}^{-1}$), which might be due to the participation of the first CF ply in the electrical conduction because of its direct contact with the NW layer. It could also be caused by the compaction of the non-woven NCCF that provides additional percolation paths in this layer; the thickness of non-woven solutions is indeed very close to that of REF material (Table III). Stacking two layers of NW0.04 further reduced the sheet resistivity (from 0.044 to 0.025 $\Omega\,\mathrm{sq}^{-1}$).

Figure 5 shows the variation of mass of REF (i.e. baseline without protection) as a function of temperature for three different heating rates, as obtained from TGA under inert atmosphere. The decomposition of the baseline starts at approximately 300°C (573 K) for a heating rate of 5 $\mathrm{K\ min^{-1}}$ and the onset temperature increases with higher heating rates. Although pyrolysis involves hundreds of reactions and intermediate species, its kinetics is often driven by a single main reaction [32]. In that case, increasing the heating rates shifts the mass with respect to temperature curves towards the right. As the heating rate during the lightning strike is much more important than those reached during TGA (probably in the order of magnitude of 10^{6}°C $\mathrm{min^{-1}}$), it is reasonable to assume that pyrolysis temperature during the lightning strike is higher than 300 °C. Nevertheless, 300 °C (573 K) will be considered to be the pyrolysis temperature in the rest of this study. The degradation mechanism of pyrolysis of epoxy resin and would be better modeled by complex reaction scheme involving intermediate reactions, but we lacked time and resources to implement it in this study, and choosing 300 °C as onset of resin pyrolysis was an acceptable compromise. The 300°C temperature will then be compared to the maximum surface temperature during lightning test. Resin pyrolysis appears to be the main cause of damages, as it triggers the production of pyrolysates, which are then trapped in the baseline. Their accumulation in the porosity increases the internal pressure, probably leading then to the material explosion.

B. Lightning tests

Figure 6 shows the recorded waveform of the current flowing in each sample during the lighting test. The peak current is always nearly the same for each solution and was measured between 35 and 37 kA. However, the decrease of the current, represented by the time to half peak in Figure 3, depends on the sample resistance: it increases with the electrical conductivity of the solution tested. This trend is observed for all samples.

Figure 7 represents the maximum temperature of each sample during the lightning tests, as measured with the infrared camera. The emissivity of the samples is very close to 0.9 for all not-painted samples and 0.92 for all painted samples. As these values did not vary significantly over the range of wavelength (from 3 to 5 μm) and temperature (300-390 K), they were considered constant during the lightning test. All temperatures saturate at the maximum temperature detectable by the camera, namely 560 K, which is very close to the pyrolysis temperature (573 K) measured by TGA shown in Figure 5. The temperature during the lightning test increases with the sample's resistivity because of the Joule effect. The saturation temperature of the camera being very close to the pyrolysis temperature, it can be observed that the unprotected panel (REF) and all the painted panels except P-ECF and P-DNW0.04 undergo pyrolysis during the lightning test. The most affected material is P-REF, as it has no protection against lightning strike. Note that the the maximum temperature of the plate during the lightning test follow the same trend as that observed on the oscilloscope, i.e. the more resistive the material is, the smaller the time to half peak is and the higher the temperature is because of the Joule Effect. Figure 8 shows the damages on the impacted zone of each solution, after lightning strike. Minor fiber breakage is visible on NW0.5 and NW0.3, while NW0.1, NW0.04, DNW0.04 and ECF show only superficial resin pyrolysis. All painted panels were severely damaged, except P-

DNW0.04 and P-ECF, which shows no significant difference with respect to ECF. Important fiber breakage is observed on P-REF, P-NW0.5, P-NW0.3 and P-NW0.1 samples, regardless of their sheet resistivity. Fiber breakage is less important on P-NW0.04, and barely visible on P-DNW0.04. No fiber breakage was observed on P-ECF. The most damaged panels are those whose temperature reached the pyrolysis temperature during the lightning tests (Figure 7), highlighting the impact of resin pyrolysis on the damage mechanism. Adhesive vaporized where the copper paths have heated on ECF. The orange and green colors observed around the impact are evidences of copper vaporization and oxidation. These results confirm the detrimental effect of the paint layer on the effectiveness of conductive coatings for LSP. They also suggest that this detrimental effect could be compensated by decreasing the sheet resistivity of the LSP.

C. Damage analysis

Figure 9 shows a typical C-Scan on a P-REF sample after lightning strike. The colors on the figure depict the decibel attenuation: red indicates unaffected zones, while blue indicates severe damages. C-Scan were performed on all solutions and the damage area was reported in Figure 10. The large error bars of these results are due to the internal delamination, which in turn depends on the explosion magnitude when pyrolysates are trapped within the plies. This phenomenon is inherently associated with a high variability as it depends on many different factors such as energy injected in the sample, sample permeability and the rate of pyrolysate production. It is difficult to clearly identify a trend because of the large variability in the measured damage area. Overall, increasing the sheet resistivity seems to reduce the area of damages, with the exception of the area of damages of NW0.5, which is smaller than that of NW0.3. However, there is no proportionality between area of damages and sheet resistivity, as the area of damages reduces only slightly between REF and ECF, while the sheet resistivity decreases by a factor of 36. The influence of the paint layer on the area of damages seems to depend on the nature of the LSP. Indeed, the area of damages decreases when REF and ECF are painted (a similar result was also observed by Kawakami and Feraboli [24]) but increases drastically when the NW are painted, with the highest values reached for P-NW 0.5. This could be due to the vaporization of the NCCF during the lightning strike, while the expanded copper foil remains stable: no significant variation was observed between ECF and P-ECF. DNW0.04 and P-DNW0.04 have the lowest area of damages among all solutions.

Figure 11 illustrates a typical CT-Scan on NW0.3 after lightning strike, showing the damages in the thickness of the composite. The CT-Scan provides a 3D reconstruction of the samples and reveals all internal damages such as broken fibers, delamination and matrix cracking. All damages are summarized in Table IV. Delamination and broken fibers were observed on all samples with various degrees of severity, except NW0.1, NW0.04, DNW0.04 and P-DNW0.04. The analysis of each slice of the sectional view allows measuring accurately the deepest damage in each sample (Figure 12). The depth of damages decreases with the sheet resistivity, showing that the LSP prevents the penetration of the damages across the thickness of the material. ECF, NW0.1 and NW0.04 were not damaged below the LSP layer. However, the depth of damages increases when the material is painted, except for ECF, which is not significantly damaged by the presence of the paint.

D. Retention of mechanical properties

Figure 13 and 14 show respectively the retention of flexural strength and modulus of elasticity in bending of each solution after lightning strike. These mechanical properties increase when the sheet resistivity of non-woven NCCF decreases, which confirms that increasing the surface conductivity of the LSP improves its efficiency [10]. NW0.1, NW0.04 and DNW0.04 reach an excellent retention of flexural strength, in the same order of magnitude than ECF, despite having a much lower weight and being cheaper (except DNW0.04 which is more expensive). Most materials have a better retention of the modulus of elasticity in bending than flexural strength, the latter being more sensitive to delamination than the modulus of elasticity in bending [33]. The retention of modulus of elasticity in bending of NW0.1, NW0.04 and DNW0.04 was close to 100%. Some of the results slightly outreached 100%, in the case of DNW0.04 and NW0.3. However, the exceeding (6%) is in the order of magnitude of the standard deviation (±7.33%) and could therefore be due to statistical margin. Another possible explanation is linked to the method of measurement. The retention was estimated by comparing a sample taken at the center of the plate, where lightning strike hits the testing panels, to samples taken closest to the edges. The mechanical properties of the corner sections could be slightly lower than the center because of the manufacturing process, although this effect is expected to be limited.

As already observed in previous works [24], [25], painting the LSP reduces a lot the retention of mechanical properties, except for P-ECF, P-NW0.04 and P-DNW0.04, which seem not significantly affected by the presence of the paint. P-NW0.04 and P-DNW0.04 have a better retention of mechanical properties than unprotected panels (REF and P-REF), so non-woven NCCF still provides a certain level of protection against lightning strike even if the material is painted. Further studies are necessary to confirm if this observation remains valid for large-scale lightning strike tests with a higher peak current. The higher sheet resistivity of the NCCF when compared to ECF could reduce its performance as LSP during a large-scale lightning test.

Figure 15 displays the retention of mechanical properties (flexural strength and modulus of elasticity in bending) as a function of the damage depth measured by CT-Scan. The retention of both flexural strength and modulus of elasticity in bending decrease in a similar extent when the depth of damage increases, showing that the mechanical properties are mainly related to the number of damaged plies. The significant reduction of mechanical properties observed on REF and all P-NW can be explained by the broken carbon fibers of the first plies, as can be seen in Figure 8. As a ply with discontinuous CF and evaporated resin cannot transmit mechanical forces, only a reduced number of plies contributes to mechanical properties. The retention of mechanical properties is therefore correlated to the depth of damages (Figure 12), which is a better indicator of the LSP efficiency than the area of damages, as already noted by Mall *et al* [13].

Overall, the error bars of the results are small, demonstrating the repeatability of the tests. Only ECF and PECF have relatively large error bars, which shows that some of the samples were more damaged than others. The reasons for this difference could not be clearly identified. The larger error bars could be due to variability in the manufacturing process of copper foils, defects in the components (resin, adhesive, copper foil) or due to some parameters specific to copper foil that could have influenced the magnitude of the explosion, for instance, the permeability.

IV. Discussion

Figure 16 illustrates the different thermal, electrical and chemical processes at stake in a composite exposed to lightning strike and leading to the damage mechanisms, for both painted and not painted materials. First, the exposed face of the composite is damaged by thermal radiation and the intense acoustic shock wave from the electric arc. Once the arc touches the composite, it expands and its diameter increases [19], affecting a wider zone (Figures 16a and b). The current flows in the LSP, but not only there: the reduction of the sheet resistivity of the LSP observed after integration on the baseline shows that the first CF plies also participate to conduction of electric current (Table III). A simple model of parallel resistances shows that the proportion of electric current that is susceptible to flow in CF plies depends on the ratio of the sheet resistivity of the LSP over the sheet resistivity of the plies: the more conductive the LSP is in comparison to CF plies, the more electric current flows in the LSP.

Then, the conduction of electric current in the LSP and carbon fibers produces Laplace force and heat through the Joule effect (Figure 16b), the latter being known to be the most important source of damage in composites exposed to lightning strikes [27]. The increase of the temperature of the polymeric resin causes its chemical degradation through pyrolysis, which produces a fragile solid compounds called "char" and emits pyrolysates [28]. These gaseous species initially accumulate in the porosity of the composite and then escape outside, if the permeability of the composite allows it (Figure 16c). However, due to the rapid nature of the lightning strike and depending on the permeability of the composite, the pyrolysates could be trapped between the plies, increasing the internal pressure in the composite and leading to delamination and explosion. The magnitude of the explosion depends on many different parameters (pyrolysate production rate, composite permeability, tensile strength of the upper plies, etc), which could explains the important variability observed in the area of damages (Figure 10). Finally, pyrolysates may contain reactive species [20] that ignite when encountering an oxidative atmosphere.

The presence of broken fibers oriented toward the outside of the composite and delamination on unprotected panels and P-NWs (Figures 8 and 11) tend to confirm the accumulation and explosion of gases between the plies. Fiber breakage is not observed on ECF, NW0.1, NW0.04, DNW0.04 and P-DNW0.04, as their lower sheet resistivity reduces Joule effect and therefore the in-depth temperature. The resin could remain below the pyrolysis temperature

(573 K for epoxy resins according to TGA data in Figure 5) or only slightly exceed it. As a consequence, the resin pyrolysis did not produce enough pyrolysates to increase the internal pressure above the threshold causing delamination or explosion. The permeability of the different LSP investigated here could also play a role, as a higher permeability could favor pyrolysates evacuation and mitigates the explosion.

Painting the composite has a detrimental effect on the efficiency of P-NW and P-DNW against lightning strike. To understand this phenomenon, it is first necessary to explain how the paint layer modifies the damage mechanism. First, the intense heat generated by the electric arc rapidly vaporizes the thin paint layer (Figure 16d). The electrical charges flow through the LSP as soon as it is revealed by the paint vaporization (Figure 16e); however, the remaining paint layer acts as an insulator and constrains the arc expansion [19]. As a result, the diameter of the electric arc on a painted material is smaller than on a material without paint, and the current density that flows in the material is much higher (Figure 16e). The first layers are vaporized more rapidly and the electrical charges are forced to travel deeper in the laminate, increasing the depth of damages (Figure 12). The Joule effect being proportional to the current density, a higher quantity of heat is produced deeper in the composite. More pyrolysates are emitted over a smaller surface, increasing the magnitude of the explosion (Figure 16f). It is worth noting that the remaining paint layer could prevent the pyrolysates evacuation and increase again the magnitude of the explosion. Typically, the failure of CFRP composites in bending purportedly occurs in three steps: first, matrix cracks may lead to interlaminar damages, then, the plies under compression might undergo buckling, and finally, the fibers could break on the tensile side [34]. Thus, there is a possibility that the resistance to tensile load of the upper ply is reduced if the fibers are broken by the lightning strike, which leads to a lower retention of mechanical properties. This explanation could suggest that the solutions with the most fiber breakage are also the ones with the most significant drop in flexural strength. Nevertheless, it is essential to acknowledge that the flexural fracture behavior of composite materials is exceedingly complex, as it can be significantly influenced by factors such as material properties, specimen geometry, and test conditions.

However, even without fiber breakage, the retention of flexural strength NW 0.1, NW 0.04 and P- DNW0.04 was respectively 84%, 85% and 87%, so slightly under the retention of the ECF (90%), probably because of the weakening of the matrix because of the high temperatures reached. Indeed, the matrix maintains the cohesion between the fibers. When a fiber break, the matrix redistributes the additional stress in the remaining fibers, which delays the rupture of the composite. However, if the matrix is damaged, the additional stress following the rupture of a fiber is transferred to the closest fibers, inducing a stress concentration and leading to a higher probability of reaching the ultimate tensile strength of another fiber, and so on. As a consequence, the retention of mechanical properties of the samples is reduced if the matrix is damaged, even if the fibers seem intact. With this regard, the adhesive surrounding the ECF protects the matrix of the composite from temperature increase. This is not the case with NCCF solutions, because the LSP is in direct contact with the matrix. The heat from Joule effect in NCCF is directly transmitted to the matrix, which can reduce the retention of flexural strength. Hence, the presence of adhesive with ECF could have a positive effect on the retention of mechanical properties after lightning strike, even if it comes with a weight penalty.

The samples protected by an expanded copper foil seem unaffected by the presence of the paint layer, while most of the samples protected by the NW are severely more damaged when painted (except P-NW0.04 and P-DNW0.04). Several hypotheses could explain this phenomenon:

- ECF has a much lower sheet resistivity than all NW solutions (Table III). Therefore, even if the current density is higher when the material is painted, the heat generated by Joule effect remains below the pyrolysis temperature (Figure 7). This hypothesis is supported by the fact that the depth of damages increases with the sheet resistivity of the LSP on P-NWs. Reducing the sheet resistivity of the LSP under the paint could help concentrate the electrical charges in the LSP and prevent them from flowing inside the plies of the composite.
- The architecture of the LSP layer could also be an important parameter, as an impermeable LSP could prevent pyrolysates from escaping and enhance the explosion. The expanded copper foil provides enough exits for the gas because of the holes between copper wires.
- The thermal conductivity of copper is more important than that of nickel, which favors heat evacuation. However, this could have a limited effect, considering the very short time scale of electric charge transfer involved in lightning strike tests.

V. Conclusion

In this study, the performances of non-woven nickel coated carbon fibers (NCCF) as lightning strike protections for composite aircraft were investigated and compared to expanded copper foil (ECF), for painted and not painted samples. The damage analysis and the measurement of the retention of mechanical properties after lightning strike showed that non-woven NCCF (NW) can provide a similar level of protection than ECF while being simultaneously lighter and cheaper than the ECF. One of the best candidate among the tested materials was the NW0.04 (non-woven NCCF with a sheet resistivity of 0.04 $\Omega\,\mathrm{sq}^{-1}$), with a retention of flexural strength of 85% without paint and 77% with paint (respectively 90 and 92% for ECF), for a lower estimated price (26% cheaper) and weight (78% lighter) than ECF. Stacking two layers of NW0.04 also allowed reaching a better retention of flexural strength (106%) than ECF, although this advantage came with a price increase (148% of the price of ECF). Painting the NW has a detrimental effect on its efficacy as a LSP, except for NW0.04, DNW0.04 and ECF, probably due to their lower sheet resistivity compared to other tested solutions. Other factors such as the architecture of the lightning strike protection and its thermal properties could play a role. A numerical model of heat transfer and chemical degradation of composite during lightning strike could help to investigate this issue and identify the most important parameters for a lightning strike protection.

The solutions developed in this research have the potential to improve the profitability of aircraft flights and reduce their emissions of pollutant by decreasing the weight of the fuselage.

VI. Fundings

This work was supported by the Natural Sciences and Engineering Research Council of Canada (NSERC) under the alliance grant ALLRP 550062 - 20 with Bell Textron Canada Ltd. The authors like to thank Bell Textron Canada Ltd for the manufacturing of the composite panels, the access to the C-scan equipment and as well as their strong technical and financial support all along the project.

VII. CRediT author statement

Jean Langot: Conceptualization, Methodology, Validation, Software, Formal Analysis, Investigation, Writing - Original Draft, Visualization.

Etienne Gourcerol: Conceptualization, Methodology, Formal Analysis, Investigation, Writing - Review & Editing.

Anamaria Serbescu: Conceptualization, Methodology, Formal Analysis, Investigation, Writing - Review & Editing.

David Brassard: Conceptualization, Methodology, Investigation, Writing - Review & Editing.

Kambiz Chizari: Conceptualization, Methodology, Writing - Review & Editing, Supervision, Project administration.

Maxime Lapalme: Conceptualization, Methodology, Validation, Resources, Supervision, Project administration.

Alexandra Desautels: Conceptualization, Methodology, Resources, Supervision.

Frédéric Sirois: Conceptualization, Methodology, Validation, Resources, Writing - Review & Editing, Supervision, Project administration.

Daniel Therriault: Conceptualization, Methodology, Validation, Resources, Writing - Review & Editing, Supervision, Project administration, Funding Acquisition.

References

[1] M. A. Uman and V. A. Rakov, "The interaction of lightning with airborne vehicles," *Progress in Aerospace Sciences*, vol. 39, no. 1, pp. 61–81, 2003.

[2] V. Mazur, *Principles of Lightning Physics*. Bristol, UKl: IOP Publishing, 2016.

[3] M. Gagné and D. Therriault, "Lightning strike protection of composites," *Progress in Aerospace Sciences*, vol. 64, pp. 1–16, 2014.

[4] B. Wang, Y. Duan, Z. Xin, X. Yao, D. Abliz, and G. Ziegmann, "Fabrication of an enriched graphene surface protection of carbon fiber/epoxy composites for lightning strike via a percolating-assisted resin film infusion method," *Composites Science and Technology*, vol. 158, pp. 51–60, 2018.

[5] J. H. Han, H. Zhang, M. J. Chen, D. Wang, Q. Liu, Q. L. Wu, and Z. Zhang, "The combination of carbon nanotube buckypaper and insulating adhesive for lightning strike protection of the carbon fiber/epoxy laminates," *Carbon*, vol. 94, pp. 101–113, 2015.

[6] P. Rajesh, F. Sirois, and D. Therriault, “Damage response of composites coated with conducting materials subjected to emulated lightning strikes,” *Materials and Design*, vol. 139, pp. 45–55, 2018.

[7] Z. Zhao, Y. Ma, Z. Yang, J. Yu, J. Wang, J. Tong, X. Yi, P. Moreira, and C. Sguazzo, “Light weight non-metallic lightning strike protection film for CFRP,” *Materials Today Communications*, vol. 25, no. July, p. 101502, 2020.

[8] K. K. Haynes, M. Clark, and A. Mazas, “Nonwoven veil technology for lightning strike protection,” *International SAMPE Symposium and Exhibition (Proceedings)*, vol. 51, 2006.

[9] Y. Guo, Y. Xu, Q. Wang, Q. Dong, X. Yi, and Y. Jia, “Eliminating lightning strike damage to carbon fiber composite structures in Zone 2 of aircraft by Ni-coated carbon fiber nonwoven veils,” *Composites Science and Technology*, vol. 169, no. 17923, pp. 95–102, 2019.

[10] J. Gou, Y. Tang, F. Liang, Z. Zhao, D. Firsich, and J. Fielding, “Carbon nanofiber paper for lightning strike protection of composite materials,” *Composites Part B: Engineering*, vol. 41, no. 2, pp. 192–198, 2010.

[11] H. Liu, Y. Guo, Y. Zhou, G. Wan, Z. Chen, and Y. Jia, “Multifunctional nickel-coated carbon fiber veil for improving both fracture toughness and electrical performance of carbon fiber/epoxy composite laminates,” *Polymer Composites*, no. July, pp. 1–13, 2021.

[12] H. Zhu, K. Fu, B. Yang, and Y. Li, “Nickel-coated nylon sandwich film for combination of lightning strike protection and electromagnetic interference shielding of CFRP composite,” *Composites Science and Technology*, vol. 207, no. January, p. 108675, 2021.

[13] S. Mall, B. L. Ouper, and J. C. Fielding, “Compression strength degradation of nanocomposites after lightning strike,” *Journal of Composite Materials*, vol. 43, no. 24, pp. 2987–3001, 2009.

[14] D. K. Chakravarthi, V. N. Khabashesku, R. Vaidyanathan, J. Blaine, S. Yarlagadda, D. Roseman, Q. Zeng, and E. V. Barrera, “Carbon fiber bismaleimide composites filled with nickel coated single walled carbon nanotubes for lightning strike protection,” *Advanced functional materials*, vol. 21, pp. 2527–2533, 2011.

[15] Q. Dong, G. Wan, Y. Xu, Y. Guo, T. Du, X. Yi, and Y. Jia, “Lightning Damage of Carbon Fiber/Epoxy Laminates with Interlayers Modified by Nickel-Coated Multi-Walled Carbon Nanotubes,” *Applied Composite Materials*, vol. 24, no. 6, pp. 1339–1351, 2017.

[16] Y. Ming, Z. Xin, Y. Zhu, C. Zhang, X. Yao, J. Sun, B. Wang, and Y. Duan, “3D printed nickel-plated carbon fiber mesh for lightning strike protection,” *Materials Letters*, vol. 294, p. 129809, 2021.

[17] J. Langot, E. Gourcerol, A. Serbescu, D. Brassard, K. Chizari, M. Lapalme, A. Desautels, F. Sirois, and D. Therriault, “A comparative study on the performance of nickel-based technologies for lightning strike protection of composite aircraft,” *ILCP*, 2022.

[18] H. Zhu, L. Chang, K. Fu, and Y. Li, “Dual conductive network of nickel-coated carbon fiber woven fabric for indirect and direct lightning strike protection of carbon fiber reinforced polymer composites,” *Polymer Composites*, vol. 43, no. 7, pp. 4437–4446, 2022.

[19] R. S. Martins, “Experimental and theoretical studies of lightning arcs and their interaction with aeronautical materials,” 2017.

[20] J. Langot, T. Pelzmann, P. Chávez-Gómez, C. S. Boanta, J. Karsten, B. Fiedler, M. Lévesque, and E. Robert, “Multi-physics modeling of the ignition of polymer matrix composites (PMCs) exposed to fire,” *Fire Safety Journal*, vol. 122, no. October 2020, 2021.

[21] A. Bigand, C. Espinosa, and J.-M. Bauchire, “Lightning Surface Explosion Impact Study On Damage Generation Into Composite,” *International Conference on Lightning & Static Electricity (ICOLSE)*, pp. 1–10, 2019.

[22] F. Moupfouma, “Aircraft Structure Paint Thickness and Lightning Swept Stroke Damages,” *SAE International Journal of Aerospace*, vol. 6, no. 2, pp. 392–398, 2013.

[23] E. Gourcerol, *Nickel coated carbon fibre nonwoven as light , efficient and scalable lightning strike protection for carbon fibre reinforced polymers Nickel coated carbon fibre nonwoven as light , efficient and scalable lightning strike protection for carbon fibre reinf*. PhD thesis, Polytechnique Montreal, 2022.

[24] H. Kawakami and P. Feraboli, “Lightning strike damage resistance and tolerance of scarf-repaired mesh-protected carbon fiber composites,” *Composites Part A: Applied Science and Manufacturing*, vol. 42, no. 9, pp. 1247–1262, 2011.

[25] V. Kumar, T. Yokozeki, T. Okada, Y. Hirano, T. Goto, T. Takahashi, A. A. Hassen, and T. Ogasawara, “Polyaniline-based all-polymeric adhesive layer: An effective lightning strike protection technology for high residual mechanical strength of CFRPs,” *Composites Science and Technology*, vol. 172, no. January, pp. 49–57, 2019.

[26] F. M. Smits, "Measurement of Sheet Resistivities with the Four-Point Probe," *Bell System Technical Journal*, vol. 37, no. 3, pp. 711–718, 1957.

[27] V. Kumar, T. Yokozeki, C. Karch, A. A. Hassen, C. J. Hershey, S. Kim, J. M. Lindahl, A. Barnes, Y. K. Bandari, and V. Kunc, "Factors affecting direct lightning strike damage to fiber reinforced composites: A review," *Composites Part B: Engineering*, vol. 183, no. December 2019, p. 107688, 2020.

[28] J. Langot, P. Chávez-Gómez, M. Lévesque, and E. Robert, "Modeling the thermal decomposition and residual mass of a carbon fiber epoxy matrix composite with a phenomenological approach: Effect of the reaction scheme," *Fire and Materials*, vol. 46, no. 1, pp. 262–276, 2022.

[29] S. M. R. Ponnada, *RESPONSE OF COMPOSITE PANELS WITH CONDUCTIVE COATINGS SUBMITTED TO EMULATED LIGHTNING STRIKES*. PhD thesis, 2017.

[30] ARP 5412B, "Aircraft Lightning Environment and Related Test Waveforms," Tech. Rep. 11, 2013.

[31] ASTM D6272, "Standard Test Method for Flexural Properties of Unreinforced and Reinforced Plastics and Electrical Insulating Materials by Four Point Bending," tech. rep., ASTM International, West Conshohocken, 2020.

[32] P. Tranchard, F. Samyn, S. Duquesne, B. Estèbe, and S. Bourbigot, "Modelling behaviour of a carbon epoxy composite exposed to fire: Part I-Characterisation of thermophysical properties," *Materials*, vol. 10, no. 5, 2017.

[33] Z. Liu, P. Li, and N. Srikanth, "Effect of delamination on the flexural response of carbon fibre reinforced polymer laminates," *Composite Structures*, vol. 209, no. October 2018, pp. 93–102, 2019.

[34] B. N. Cox, M. S. Dadkhah, W. L. Morris, and J. G. Flintoff, "Failure mechanisms of 3D woven composites in tension, compression, and bending," *Acta Metallurgica Et Materialia*, vol. 42, no. 12, pp. 3967–3984, 1994.

[35] "The Engineering Toolbox," *https://www.engineeringtoolbox.com/*, 2023.

[36] "Markets Insider," *https://markets.businessinsider.com/commodities*, 2022.

[37] A. S. S. D. Association, "Galvanic series," *https://www.assda.asn.au/*, 2022.

VIII. FIGURES

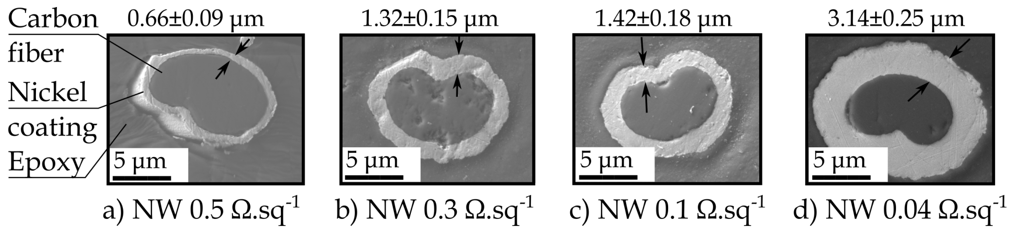

Fig. 1. Magnified view obtained with SM 7600 TFE Scanning Electron Microscope, showing a cross-sectional view of a single nickel coated carbon fiber on non-woven NCCF with sheet resistivity of a) 0.5 $\Omega\,\mathrm{sq}^{-1}$, b) 0.3 $\Omega\,\mathrm{sq}^{-1}$, c) 0.1 $\Omega\,\mathrm{sq}^{-1}$ and d) 0.04 $\Omega\,\mathrm{sq}^{-1}$ (Fig d)).

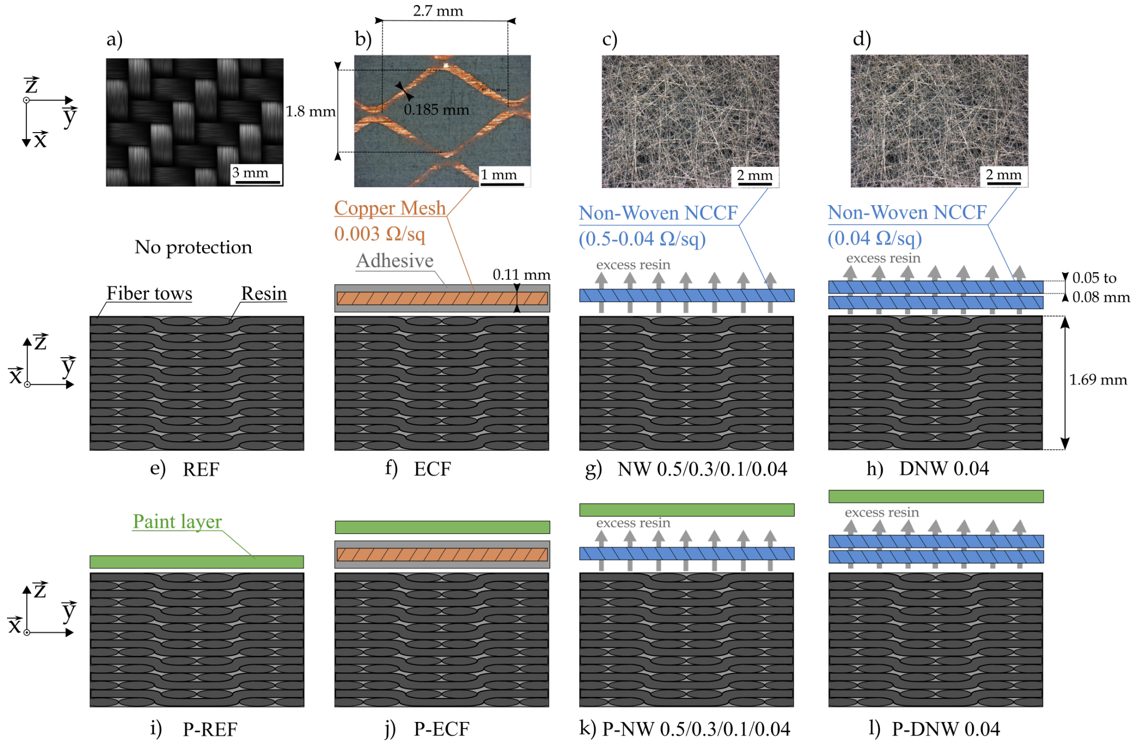

Fig. 2. Schematics and images of the samples studied in the research. a) Top view of a typical carbon fiber ply used in the baseline material. b) Optical image of copper foil embedded in adhesive (top view). c) and d) Optical images of non-woven nickel coated carbon fibers (0.1 $\Omega\,\mathrm{sq}^{-1}$, top view). e) REF: baseline material (carbon fibers and epoxy matrix) without any LSP (sectional view). f) ECF: baseline protected by an expanded copper foil (sectional view). g) NW 0.5/0.3/0.1/0.04: baseline protected by one layer of Non-Woven NCCF, with sheet resistivity of 0.5, 0.3, 0.1 or 0.04 $\Omega\,\mathrm{sq}^{-1}$ (sectional view). h) DNW 0.04: baseline protected by two layers of Non-Woven NCCF, with sheet resistivity of 0.04 $\Omega\,\mathrm{sq}^{-1}$ (sectional view). i) P-REF: REF with a paint layer on top (sectional view). j) P-ECF: ECF with a paint layer on top (sectional view). k) P-NW 0.5/0.3/0.1/0.04: NW0.5/0.3/0.1/0.04 with a paint layer on top (sectional view). k) P-DNW 0.04: DNW 0.04 with a paint layer on top (sectional view).

497

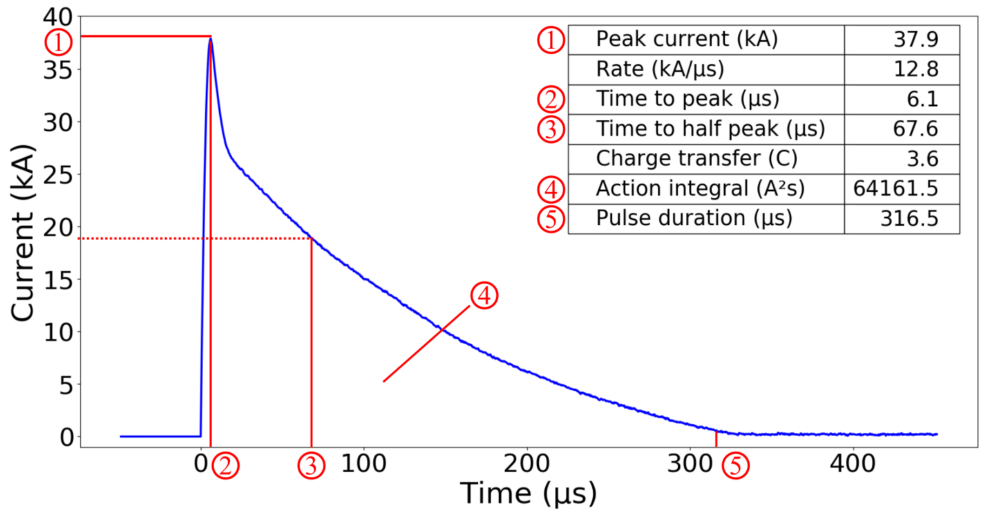

Fig. 3. A typical current vs time A-component like waveform on ECF produced with the lightning strike emulator developed at Polytechnique Montreal. [17]

498

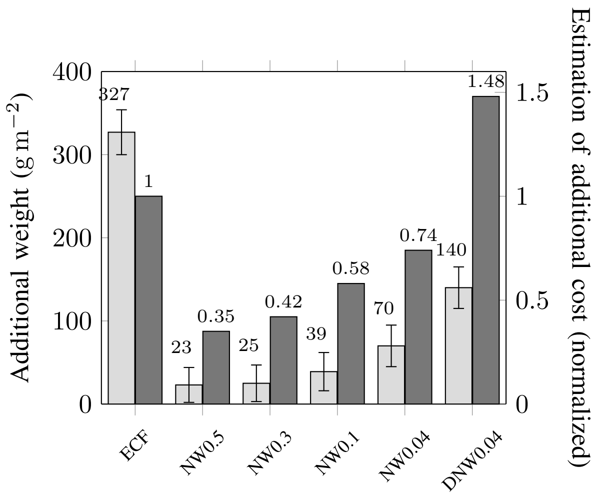

Fig. 4. : Additional weight of each solution (left y-axis). : Relative additional cost of each solution (right y-axis), normalized with respect to ECF's price. The error bars are the standard deviation.

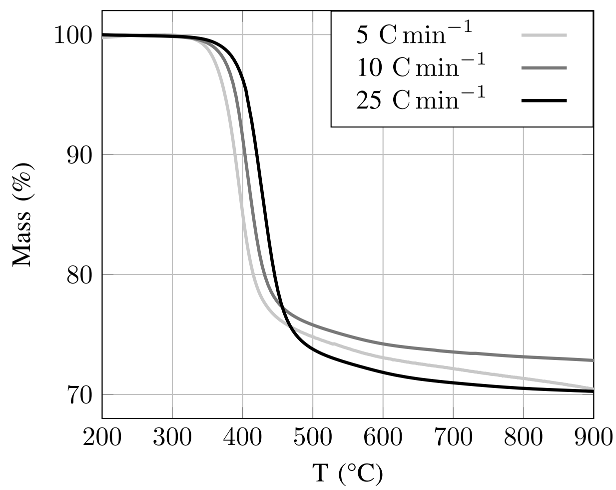

Fig. 5. Thermogravimetric analysis of REF (carbon fiber epoxy matrix composite with no LSP) under inert atmosphere (N_2).

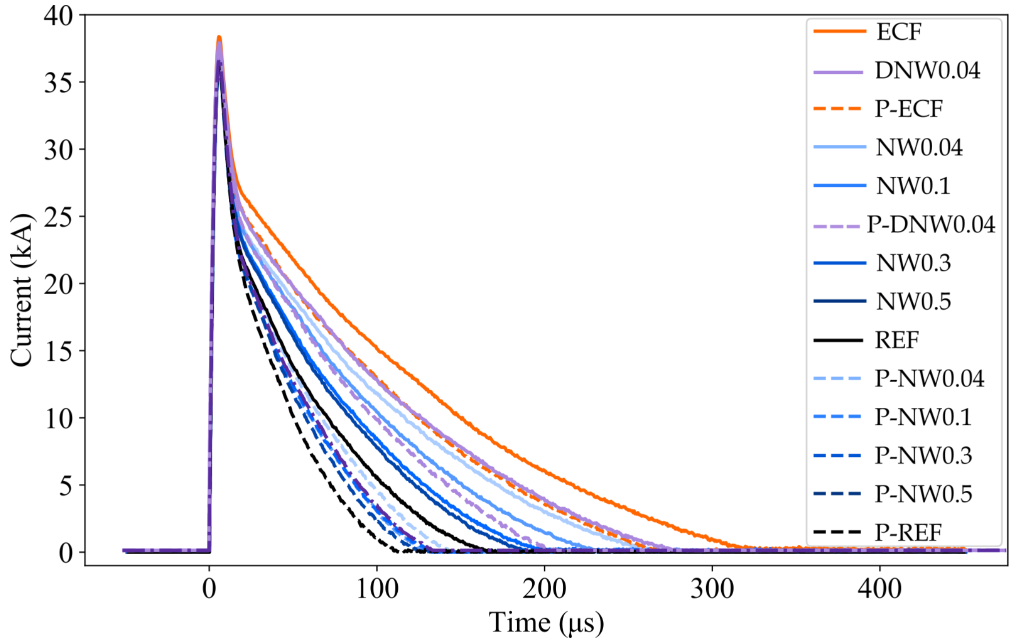

Fig. 6. Current waveforms of each sample during the lighting strike test.

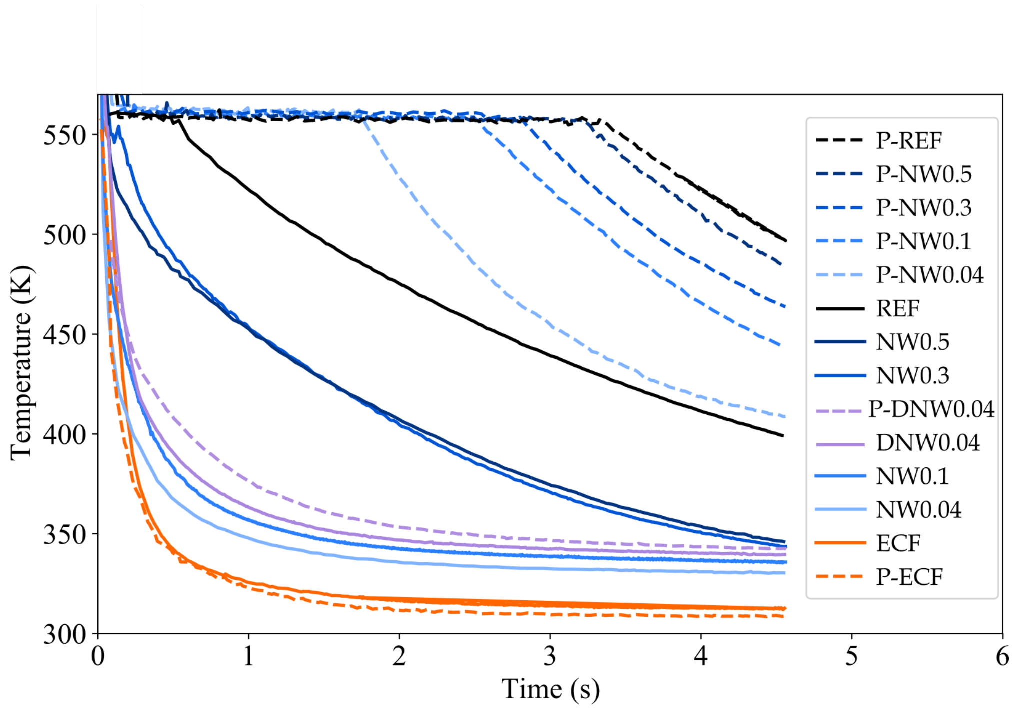

Fig. 7. Maximum surface temperature of each sample during lightning strike tests, as measured with an infrared camera. The saturation temperature of the camera is 560 K. The recording ends 4.5 seconds after the lightning strike.

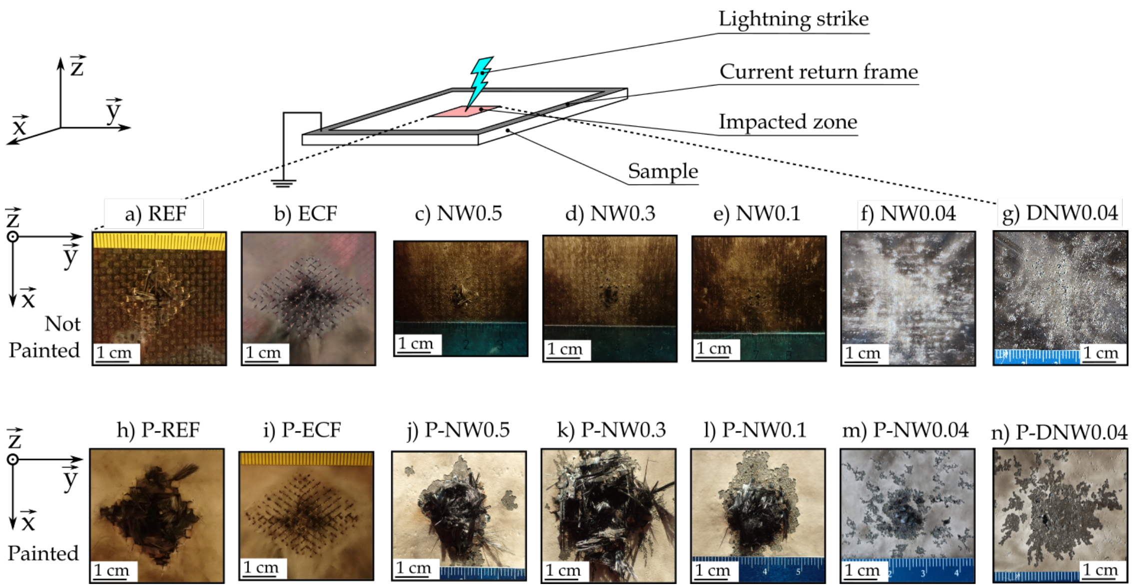

Fig. 8. Close-up views of the damages on not painted (a-g) and painted (h-n) samples after lightning strike tests.

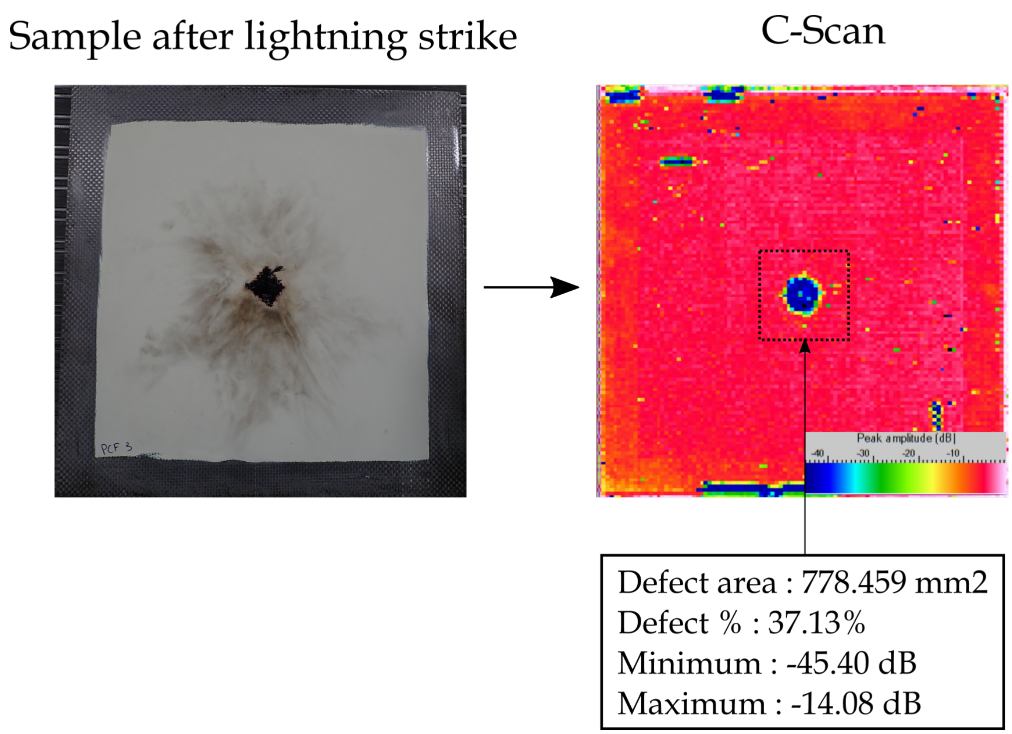

Fig. 9. A typical C-Scan on a P-REF after lightning strike tests.

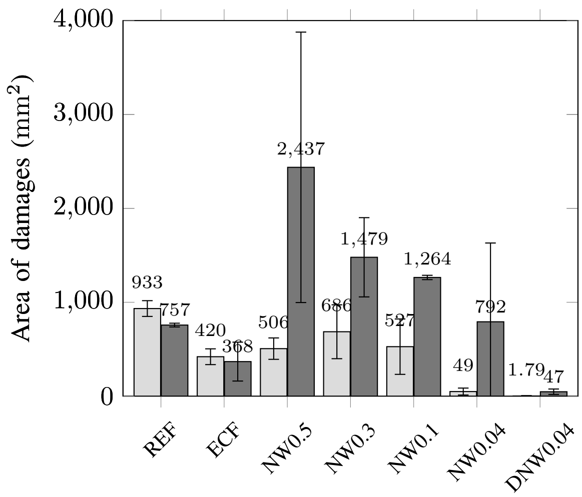

Fig. 10. Area of Damages of each not painted ( ) and painted ( ) solutions, measured by C-Scan. The error bars indicate the standard deviation.

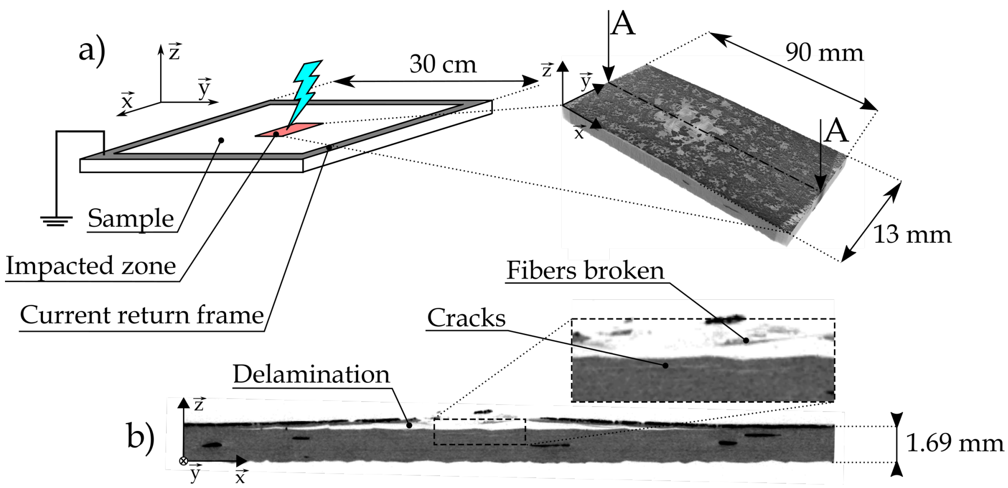

Fig. 11. CT-Scan of NW0.3 (as an example) after lightning strike. a) Schematic showing the localisation of the zone inspected by CT-Scan and isometric view of NW0.3. b) Sectional view (A-A) of the damages inside NW0.3.

503

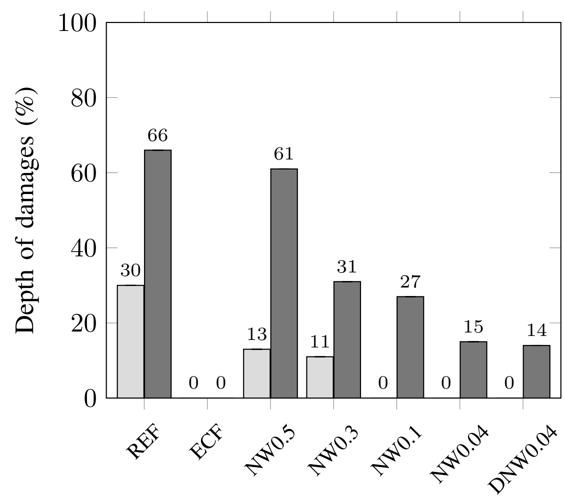

Fig. 12. Depth of Damages of each not painted ( ) and painted ( ) solutions, observed on CT-Scan images.

504

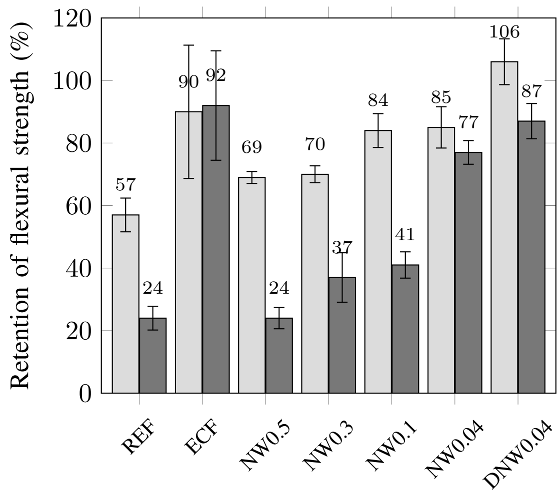

Fig. 13. Retention of flexural strength of each non-painted ( ) and painted ( ) solutions, measured by 4-point bending tests. The error bars indicate the standard deviation.

505

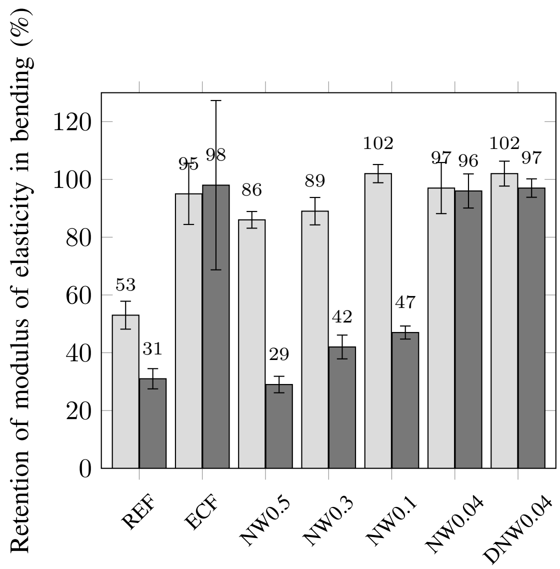

Fig. 14. Retention of the modulus of elasticity in bending of each non-painted ( ) or painted ( ) solutions, measured by 4-point bending tests. The error bars indicate the standard deviation.

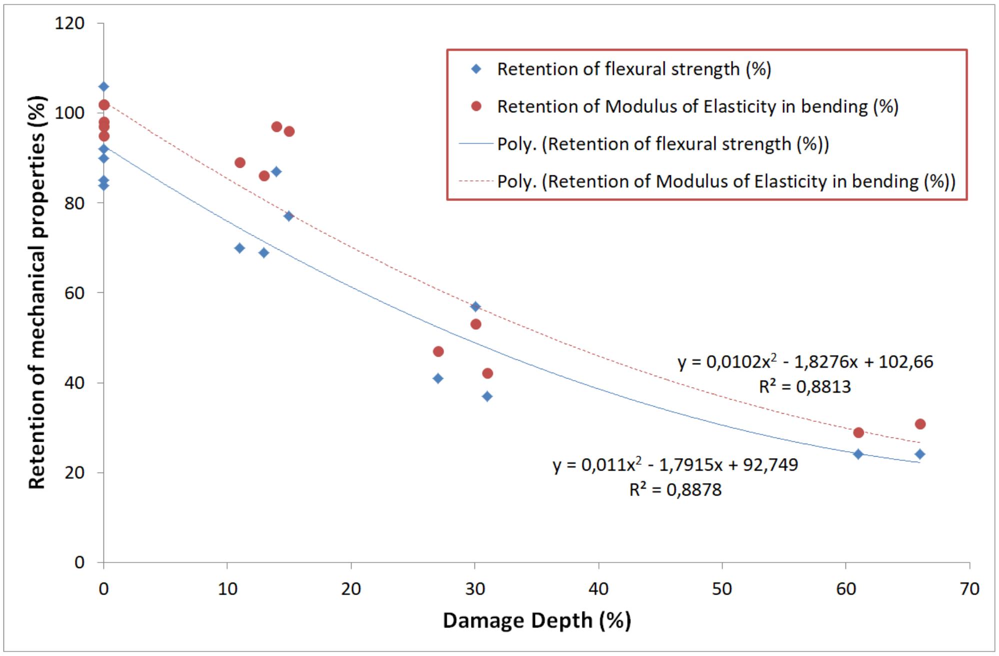

Fig. 15. Retention of the mechanical properties as a function of the damage depth in the laminate, in percentage. The continuous line depicts the polynomial interpolation of the retention of flexural strength, and the dashed line depicts the polynomial interpolation of the retention of modulus of elasticity in bending.

507

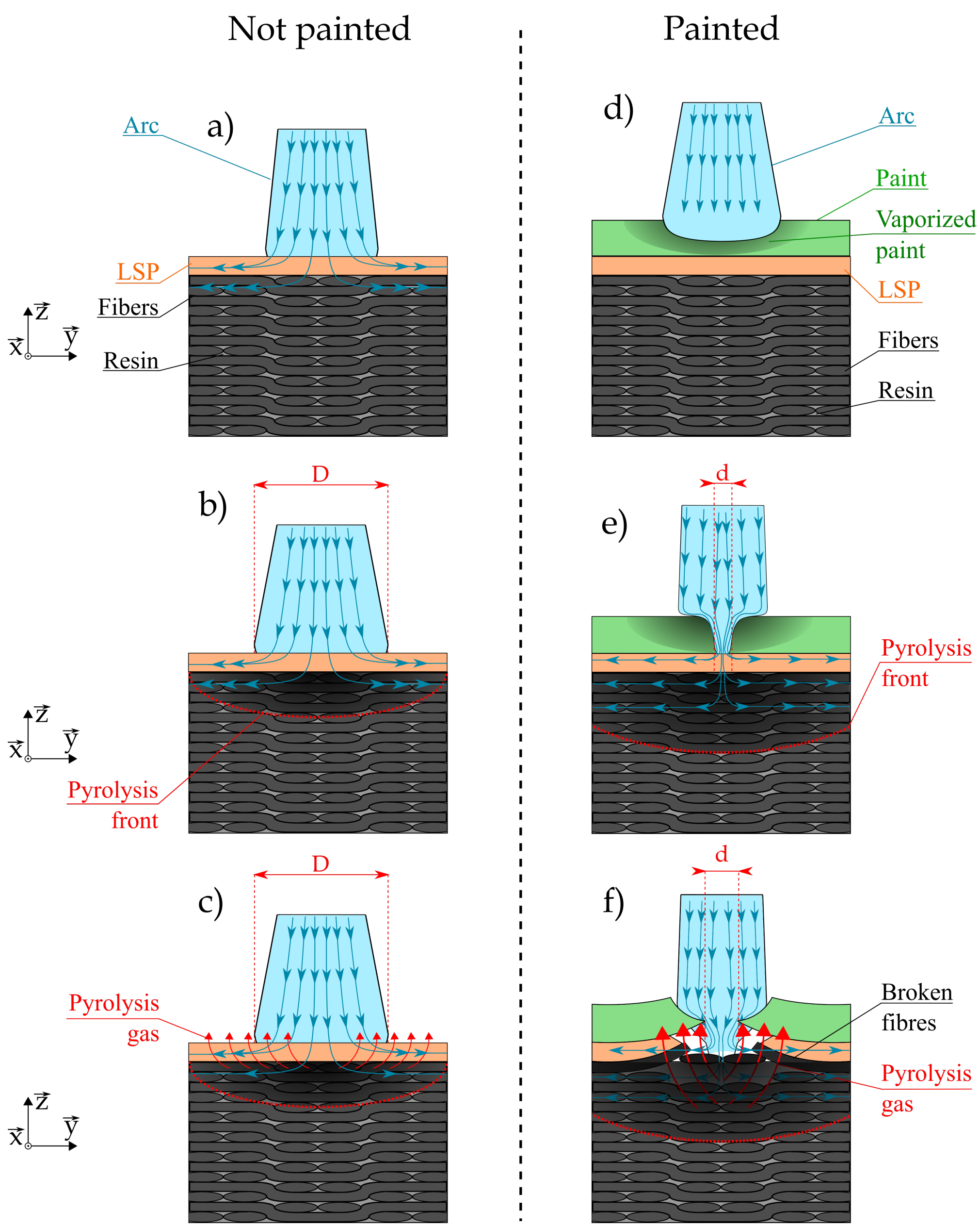

Fig. 16. Damage mechanisms during a lightning strike on non-painted and painted CFRP laminates. a) to c): damage mechanisms in a composite panel protected by a LSP, not painted. a) Attachement of the lightning to the LSP and conduction in the LSP and in the composite. b) Heating of the matrix because of Joule effect and progression of a pyrolysis front. c) Evacuation of the pyrolysis gases through the upper layers. d) to f) Damage mechanisms in a painted composite panel protected by a LSP. d) Vaporization of the paint layer by the lightning arc. e) Conduction in the LSP and composite as soon as the lightning reaches the LSP, and creation of a pyrolysis front. The diameter of the arc root is smaller than in b) because of the paint layer, so the current density is higher and the electric current flows deeper in the composite. f) Increase of the of the internal pressure because of the pyrolysis gases trapped between the plies, until explosion.

508

IX. Tables

TABLE I

MAIN PROPERTIES OF COPPER AND NICKEL [35]. THE PRICES ARE INDICATED AS FOR JANUARY 2022 [36]. THE RELATIVE MAGNETIC PERMEABILITY INDICATE THE PERMEABILITY OF A MEDIUM RELATIVELY TO FREE SPACE.

Material	Density ($kg\,m^{-3}$)	Price ($\$\,kg^{-1}$)	Electrical conductivity (S/m)	Anodic index (V) [37]	Relative magnetic Permeability (-)	Temperature (°C)		Latent heat (kJ/mol)	
						Fusion	Vaporization	Fusion	Vaporization
Copper	8960	9.76	5.96×10^7	-0.35	1	1085	2562	13.26	300.4
Nickel	8910	24.3	1.44×10^7	-0.30	100-600	1455	2730	17.48	379

TABLE II

PROPERTIES OF THE ECF

Thickness (mm)	Areal weight of copper mesh ($g\,m^{-2}$)	Areal weight of adhesive ($g\,m^{-2}$)	Type of Adhesive	Curing
0.11	146	181	Epoxy	177°C

TABLE III

SURFACE RESISTIVITY AND THICKNESS OF ALL SOLUTIONS BEFORE PAINTING. THE SHEET RESISTIVITY OF THE DNW0.04 BEFORE INTEGRATION CORRESPONDS TO THE SHEET RESISTIVITY OF A SINGLE VEIL OF NW NCCF OF $0.04\ \Omega\,sq^{-1}$. THE ERROR INDICATED IS THE STANDARD DEVIATION.

Sample	REF	ECF	NW0.5	NW0.3	NW0.1	NW0.04	DNW0.04
Sheet resistivity ($\Omega\,sq^{-1}$) **before** integration	-	-	0.430±0.047	0.267±0.026	0.124±0.009	0.045±0.003	0.045±0.003
Sheet resistivity ($\Omega\,sq^{-1}$) **after** integration	0.250±0.072	0.003±0.001	0.175±0.025	0.132±0.013	0.062±0.008	0.044±0.004	0.025±0.005
Total thickness (mm)	1.69±0.01	1.83±0.02	1.70±0.01	1.69±0.01	1.69±0.01	1.69±0.01	1.70±0.01

TABLE IV
LIST OF THE DAMAGES OBSERVED VISUALLY AND WITH THE CT-SCAN, ON EACH SOLUTION.

Solution	Damages to LSP	Matrix cracking	Delamination (number of plies)	Fibers broken
REF	-	Yes	2	Very important
ECF	Melted at crosspoints and partially vaporized	No	0	No
NW0.5	Vaporized under impact and at crosspoints of fiber tows	Yes	1	Important
NW0.3	Vaporized under impact and at crosspoints of fiber tows	Yes	1	Marginal
NW0.1	Vaporized at crosspoints of fiber tow	Yes	0	No
NW0.04	Partially vaporized	No	0	No
DNW0.04	Slightly vaporized	No	0	No
P-REF	-	Yes	5	Very important
P-ECF	Melted at crosspoints and partially vaporized	No	0	No
P-NW0.5	Vaporized under impact	Yes	5	Very important
P-NW0.3	Vaporized under impact	Yes	2-3	Very important
P-NW0.1	Vaporized under impact	Yes	2-3	Important
P-NW0.04	Vaporized under impact	Yes	1	Marginal
P-DNW0.04	Vaporized at crosspoints of fiber tows	Yes	1	No